Journal of Applied Physics

RESEARCH ARTICLE | FEBRUARY 14 2024

Impact of the thickness on the optical and electronic and structural properties of sputtered Cu_2S thin films

J. R. Velasquez-Ordoñez ; J. Rivera-Taco ; D. G. Pacheco-Salazar ; J. A. H. Coaquira ; J. L. Maldonado ; J. A. Guerra ; P. Llontop ; P. C. Morais ; F. F. H. Aragón

J. Appl. Phys. 135, 065703 (2024)
https://doi.org/10.1063/5.0191049

Journal of Applied Physics ARTICLE pubs.aip.org/aip/jap

Impact of the thickness on the optical and electronic and structural properties of sputtered Cu_2S thin films

Cite as: J. Appl. Phys. **135**, 065703 (2024); doi: 10.1063/5.0191049
Submitted: 11 December 2023 · Accepted: 14 January 2024 ·
Published Online: 14 February 2024

J. R. Velasquez-Ordoñez,[1] J. Rivera-Taco,[1] D. G. Pacheco-Salazar,[1] J. A. H. Coaquira,[2] J. L. Maldonado,[3] J. A. Guerra,[4] P. Llontop,[4] P. C. Morais,[2,5] and F. F. H. Aragón[2,a)]

AFFILIATIONS

[1]Laboratorio de Películas Delgadas y Nanomateriales, Escuela Profesional de Física, Universidad Nacional de San Agustín de Arequipa, Arequipa, Peru
[2]Núcleo de Física Aplicada, Instituto de Física, Universidade de Brasília, Brasília DF 70910-900, Brazil
[3]Research Group of Optical Properties of Materials (GPOM), Centro de Investigaciones en Óptica, A.C. 1-948, Loma del Bosque 115, León 37150, Guanajuato, Mexico
[4]Departamento de Ciencias, Sección Física, Pontificia Universidad Católica del Perú, Av. Universitaria1801, San Miguel, Lima 32, Peru
[5]Genomic Sciences and Biotechnology, Catholic University of Brasília, Brasília DF 70790-160, Brazil

[a)]**Author to whom correspondence should be addressed:** ffharagon@gmail.com

ABSTRACT

A successful hexagonal Cu_2S p-type semiconductor thin film using DC magnetron sputtering is reported. Films with thickness gradients were deposited by taking advantage of deposition geometry and target dimensions. X-ray diffraction (XRD) analysis confirmed the exclusive formation of the hexagonal Cu_2S phase. Elemental composition and thickness dependence with the sample position were determined using energy-dispersive x-ray spectroscopy. Optical properties, including the optical bandgap, refractive index, and extinction coefficient, were assessed by modeling transmittance spectra. The Tauc–Lorentz oscillator and Drude models were employed for this purpose. XRD data analysis successfully determined the film thickness (t_{XRD}) as a function of the sample position, aligning well with thickness values (t_T) derived from transmittance spectra analyses. These results were further supported by film thickness values (t_{SEM}) obtained from cross-sectional SEM images. Charge carrier density and mobility, extracted from the optical models, were found to be consistent with DC electrical measurements. AC impedance curves were effectively modeled with RL–RC parallel circuits. The results indicate that the inductance (L) and capacitance (C) components of the films increase with decreasing film thickness.

I. INTRODUCTION

In the coming years, the global demand for renewable energies will certainly witness an increase. This is primarily because most of the energy used nowadays comes from the combustion of fossil fuels (non-renewable energy), which has been pointed out as highly harmful to the climate and living beings. In this context, although silicon is one of the most common elements on the planet,[1] its production process for solar cells (better than 99.99% purity) is expensive,[2] thus the search for alternative materials with easier and cheaper manufacturing techniques is still necessary. In this context, p-type transparent conducting materials (TCMs) are essential for the production of inorganic solar cells. The Cu_2S hexagonal phase has a hole concentration in the range of $\sim 1.2 \times 10^{20}$ -1.6×10^{22} cm^{-3} (Ref. 3) and bandgap energy (E_g) in the range of 1.2–2.5 eV,[4] making this a worthwhile option for TCMs. The hexagonal phase is one of the five more stable phases at room temperature.[5] Regarding the production of this material, different techniques for the deposition of copper sulfide thin films are reported in the literature,

between them, one can highlight the hydro- and solvothermal,[6] thermionic vacuum arc,[7] vacuum thermal evaporation,[3] reactive sputtering,[8] and the reactive radio frequency (RF) sputtering method.[9] However, it should be noted that the growth conditions on the magnetron sputtering system, such as the deposition rate, substrate type, work pressure, magnetic field configuration, and temperature of the substrate lead to a significant impact on the resulting feature Cu_2S thin film. In particular, a slight change in film's stoichiometry could lead to a polymorphism change. On the other hand, a crucial point in the development of new optoelectronic devices is to understand the thickness distribution while employing magnetron sputtering, where parameters such as source design, target erosion, and source-to-substrate distance promote changes in the thickness distribution.[10] The film thickness, which is usually regulated by the deposition time,[11,12] and the growth rate, which is tightly controlled by the power in sputtering deposition,[13] have a significant impact on the final properties of Cu_2S films. The physical properties of the film are closely related to its thickness. A substantial reduction in film thickness can cause a quantum confinement effect by changing the grain size of the crystal. Beyond this, reduction in film thickness causes strain at the film's surface and interface by increasing the surface area while also introducing asymmetry. These effects display the close relationship between the structural, optical, and electric properties of the film. Several methods are available for measuring the films' thickness, for example, the examination of the cross section for instance, the most commonly used one. However, evaluating the film cross section is an expensive and destructive method. Additionally, in films with a depth gradient, the thickness of a specific region of the sample could diverge from the average values. Here, the optical methods provide larger spots and potentially more accurate readings. Nevertheless, due to the numerous parameters required for modeling the optical dispersion, it may be difficult to conduct proper analyses. An alternative method is x-ray reflectometry (XRR), however, not all laboratories have access to this type of analysis. A tentative approach was made by Srinivasan *et al.,* who used a conventional x-ray diffraction (XRD) method to measure the thickness of nickel deposits on mild steel plates and compared their findings with those from weighing and metallographic examination.[14] Despite satisfactory results, to our knowledge, no additional research has been conducted on this subject.

In this work, we present the growth of hexagonal Cu_2S thin films, along with a comprehensive structural, optical, and electrical characterization. Our investigation reveals a strong correlation between the thickness gradient and the substrate position. This correlation is determined through conventional XRD patterns and optical analysis. Additionally, it is further supported by cross-sectional micrographs. These findings allow us to evaluate the impact of material thickness on the structural, optical, and electrical properties of the films. A noteworthy outcome of our study is the determination of carrier concentration and mobility, achieved through optical characterization and validated by Hall effect measurements. We believe that these findings contribute to a deeper understanding of the material's properties and its potential applications.

II. EXPERIMENTAL DETAILS

Copper sulfide thin film deposition was carried out onto glass substrates (borosilicate) via DC sputtering at room temperature.

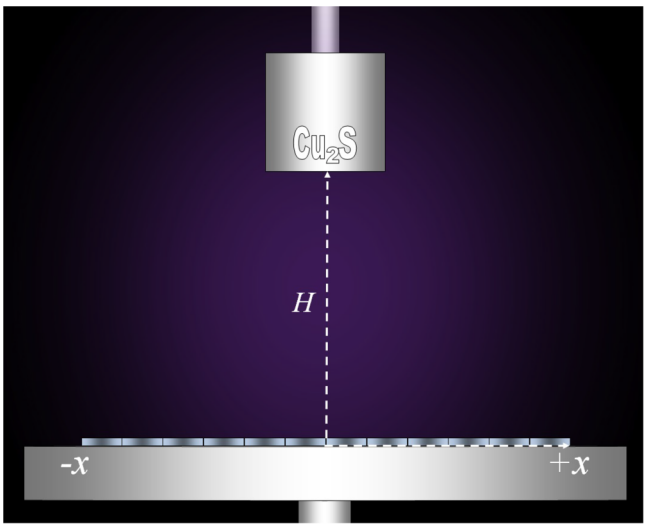

FIG. 1. Schematic representation of the distance (x) on the as-grown Cu_2S thin film used to obtain the XRD pattern.

Films with different thicknesses were obtained by distributing glass substrates with $10 \times 10\ mm^2$ dimensions one aside the other along the $\pm x$ axis, where x is the position of one of the substrates measured from the center ($x = 0$), which goes up to $\pm$ 55 mm. Previously, the substrates were carefully cleaned by soaking in soapy water and sonicating for 20 min, following cleaning with distilled water, repeating the procedure with isopropyl alcohol, and, finally, drying in hot air. The magnetron sputtering configuration was designed for the growth of the films, with substrate to target distance set at 50 mm while controlling the deposition rate via the DC power supply (12 W), with deposition time set for 60 min. The base pressure and work pressure were set at 4.2×10^{-5} and 5.5×10^{-3} mbar, respectively. The latter is controlled by the high-purity argon gas flow into the vacuum chamber. The configuration of the samples is located in a line moving away from the center, toward the positive and negative direction along the x-axis according to Fig. 1.

The latter was employed during the deposition process to adjust the thickness of the layers. A Rigaku-Miniflex 600 x-ray diffractometer equipped with a copper anode was used for structural characterization. Diffraction patterns were analyzed using the Rietveld refinement method implemented in the Generalized Structure Analysis System (GSAS).[15] The film resistivity, sheet resistance, and carrier concentration were measured using the standard Van Der Pauw configuration for Hall effect measurements. Optical characterization was assessed through transmission measurements performed with a UV-1800 model SHIMADZU spectrometer, in the wavelength range from 190 to 1100 nm, using a deuterium lamp (UV light) and tungsten lamp (visible light) as light sources. The cross-section images were obtained using a JEOL Scanning Electron Microscopy (SEM) model JSM 7001F operating at 10 kV. The AC electrical measurements were recorded using a HP 4284A system operating in the frequency range from 20 Hz to 1 MHz.

III. EXPERIMENTAL RESULTS AND DISCUSSION

1. Structural properties

Figures 2(a) and 2(b) show the XRD patterns for the as-grown polycrystalline Cu_2S films corresponding to different regions along the x-axis. Those regions were defined according to the distance from the center of the supporting substrate ($x = \pm 5, \pm 15, \pm 25, \pm 35, \pm 45, \pm 55$ mm). As indicated in Fig. 1, the distance between the target and the substrate center was H = 50 mm. As can be inferred from the plots in Figs. 2(a) and 2(b), the intensity of every XRD peak has a strong correlation with the distance (x) and the mean film thickness. The XRD peaks were indexed as the Cu_2S hexagonal phase, with space group P63/mmc. Analysis of the XRD data indicates the formation of only hexagonal Cu_2S, with no evidence of other crystalline or amorphous phase besides the borosilicate glass substrate characterized by a broad band located ~25° [see Figs. 2(a) and 2(b)]. To assess the structural properties of as-grown Cu_2S films, the XRD patterns were further analyzed by the Rietveld refinement method. For the refinements, the Lorentzian function $H_L = X\tan\theta + Y/\cos\theta$ was used to model the peak shape, where X and Y are the refinable parameters. Table I shows the lattice constant values ($a = b$ and c) obtained from the fitting procedure, and it shows that the lattice constant values reveal a slight tendency to increase as the analyzed region approaches the sample holder center (lower x values). The latter can be easily verified in the plot of the unit cell volume (V) against x, as shown in Fig. 3(a). This systematic trend is herein related to the compression strained states in the region far from the center (thinner film), which then relax as the x position is closer to the sample holder's center, approaching the value reported by Cava *et al.* for hexagonal Cu_2S single-crystal using neutron diffraction data.[16] The mean crystallite size $\langle D\rangle$ was calculated using the Scherrer equation, $\langle D\rangle = k\lambda/(\beta_{size}\cos\theta)$, where k is the Scherrer constant, λ is the wavelength of the x-ray beam used (0.154 nm), $\beta_{size} = \beta_{exp} - \beta_{inst}$ is the corrected full width at half maximum (FWHM) of the XRD peak of the diffraction peak width measurement (β_{exp}) and the instrumental broadening (β_{inst}) contribution, and θ is Bragg's angle.[17]

As shown in Table I, the $\langle D\rangle$ parameter displays higher values in the thicker region of the film (lower x distance) and a decreasing tendency in the thinner region of the film (higher x distance),

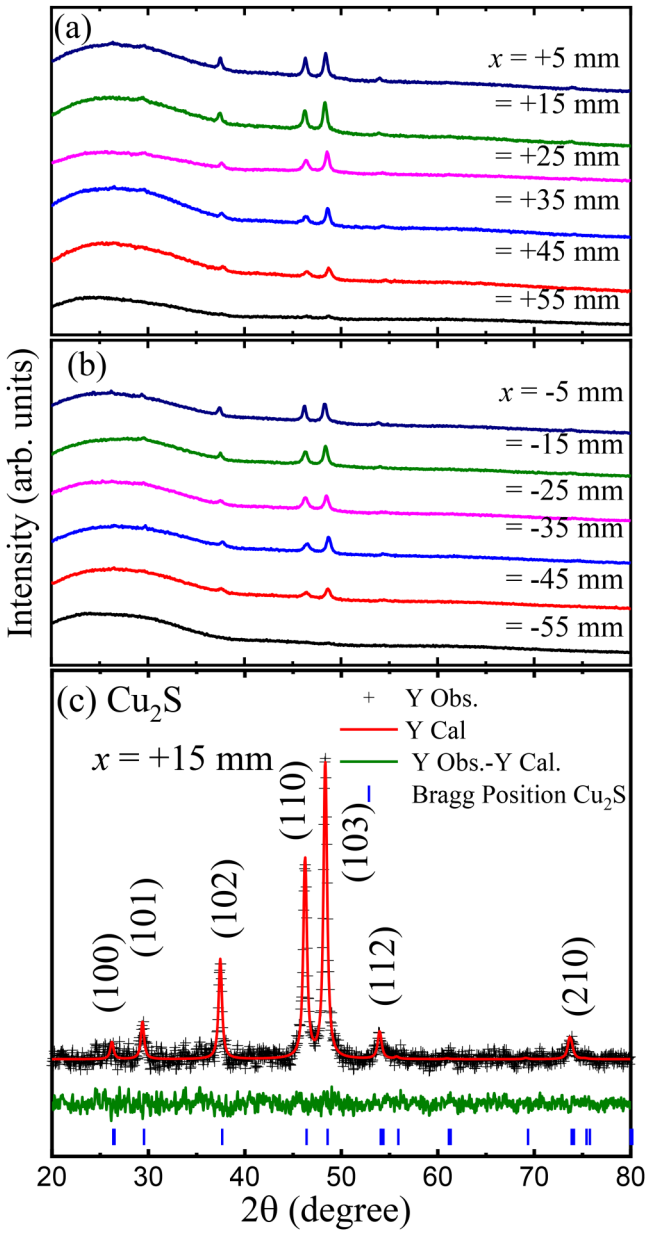

FIG. 2. (XRD patterns recorded from regions located at different distances (x) from the center of the substrate toward (a) right and (b) left. (c) Refined XRD pattern, which corresponds to the film region located at $x = +15$ mm from the center. Symbols in (c) represent experimental data; the solid red line is the calculated data, and the solid green line is the difference between them. The blue ticks at the bottom of the panel represent the expected positions of Bragg's reflections.

TABLE I. List of the structural parameters of the Cu_2S thin film extracted from the XRD Rietveld refinement. The S-factors (R_{wp}/R_{exp}) indicate the quality of the refinement. The film's thickness (t_{XRD}) was determined according to the provided in the text.

x (mm)	a (Å)	c (Å)	V(Å^3)	$\langle D\rangle$ (nm)	S	t_{XRD} (nm)
−55	3.907	6.729	88.979	…	1.31	153 ± 40
−45	3.914	6.735	89.348	17 ± 1	1.31	646 ± 100
−35	3.906	6.726	88.895	19 ± 1	1.33	963 ± 200
−25	3.921	6.757	89.952	17 ± 1	1.29	969 ± 40
−15	3.922	6.773	90.205	20 ± 1	1.27	1052 ± 100
−5	3.929	6.783	90.701	24 ± 1	1.31	936 ± 200
+5	3.922	6.773	90.225	23 ± 1	1.29	953 ± 80
+15	3.926	6.783	90.561	21 ± 1	1.28	1026 ± 100
+25	3.916	6.747	89.603	20 ± 1	1.27	1165 ± 90
+35	3.915	6.738	89.459	21 ± 1	1.30	742 ± 70
+45	3.906	6.720	88.809	17 ± 1	1.29	580 ± 60
+55	3.914	6.723	89.193	…	1.27	196 ± 60

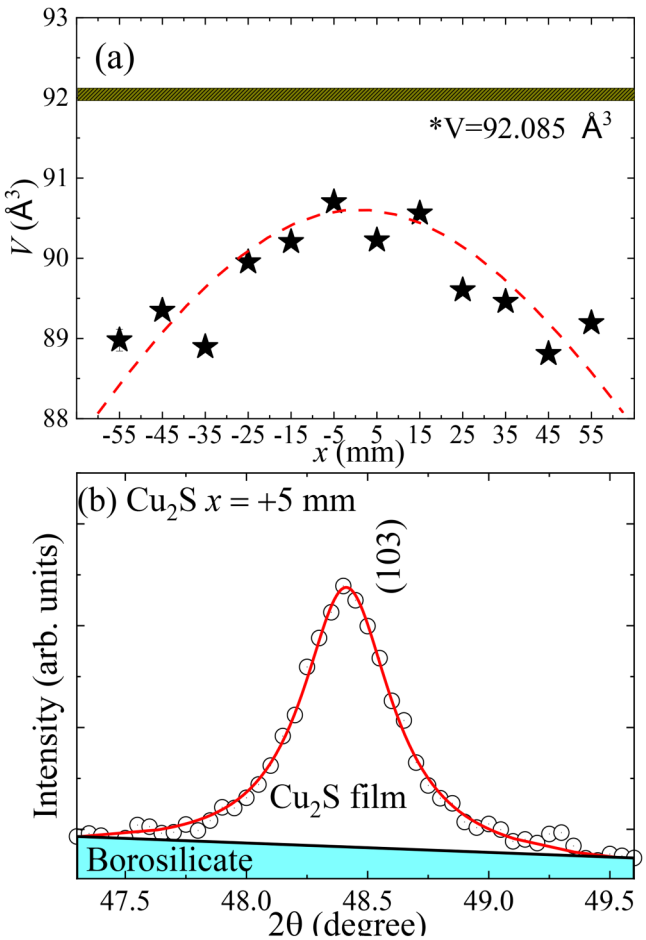

FIG. 3. (a) Unit cell volume vs the distance (x) from the center of the substrate. The dashed red line is only a guide to the eyes (Ref. 16). (b) (103) Bragg peak: the open circles represent the experimental data and the solid red line represents the data fit using the Lorentzian peak-shape function.

despite the general understanding that film thickness and crystallite mean size relationship is complex and depends on multiple factors, such as strain effects, surface energy, growth mode, surface and interface effects, or combination of multiple factors. Therefore, it is essential to consider that in the sputtering technique, the growth process is governed by island formation. In the early stages of growth, islands of crystalline material may form on the substrate. The size and density of these islands can affect the overall crystallite size within the end film. Thicker films may have more time for these islands to coalesce and grow, leading to larger crystallite sizes. The increase in the film's thickness is largely reported in the literature, in which it is claimed that the crystallite size within the film increases with the film thickness.[18,19]

The x-ray diffraction data can be used to estimate the film thickness, given that the XRD pattern includes information about the substrate and the deposited film on top of it. In this regard, the estimation of the film thickness is based on the observed change in the x-ray absorption of the film, assuming that the crystallites in the film are randomly oriented, as reported by Srinivasan *et al.*.[14] The thickness (t_{XRD}) of the deposited film can be obtained from the XRD diffraction peak through the relationship between the peak area of the uncoated substrate (A_s) and the peak area of the coated substrate, i.e., including the film on top of the substrate [$A_{film} = A_s$ + Area above in Fig. 3(b)]. Equation (1) describes the relationship between A_{film} and A_s, assuming that the substrate is significantly thicker than the film and that the sample's absorption increases with the amount of the material,

$$A_{film} = A_s e^{-(2\mu_{film} t_{XRD} \operatorname{cosec}\theta)} \tag{1}$$

where $e^{-(2\mu_{film} t_{XRD} \operatorname{cosec}\theta)}$ is an attenuation factor produced by the film with a thickness t_{XRD}, whereas μ_{film} is the linear absorption coefficient of the material. The linear absorption coefficient of the hexagonal Cu_2S is 337 cm^{-1}.[20] The thickness of the film (t_{XRD}) can be obtained from Eq. (2),

$$t_{XRD} = \frac{1}{2\mu_{film} \operatorname{cosec}\theta} \left| \ln\left(\frac{A_s}{A_{film}}\right) \right|. \tag{2}$$

Figure 3(b) depicts the best fitting of the (103) XRD peak using the Lorentzian peak-shape function to assess the uncoated and coated substrate area within the corresponding Bragg angle range. To increase the accuracy, two XRD peaks (110 and 103) were used in the analysis. The average values of the film thickness at each distance (x) are collected in Table I and graphically displayed in Fig. 6(a). Our findings indicate a maximum value of t_{XRD} for x around 25 mm, which may be explained by the target's erosion pattern, caused by the magnetic sputtering setup. Moreover, the maximum value of t_{XRD} is observed in the positive and negative distances (x), roughly symmetrically, which is closely linked to the source-to-substrate distance according to simulations using target erosion data.[10]

2. Morphological characterization

As shown in Figs. 4(a) and 4(b), the cross-sectional SEM images show that the film thickness tends to decrease as the distance (x) increases, i.e., going away from the center of the substrate. Additionally, a dense and uniform film is observed at each particular distance (x). However, because the deposited film is expected to show a thickness dependence on x (thickness gradient), this may lead to a misinterpretation of the film's average thickness value. Nevertheless, depending on the distance (x) where the analysis is performed, this could not always be the most representative value as it will be discussed later on in this report. Moreover, to make a qualitative elemental characterization of the as-grown film, energy-dispersive x-ray spectroscopy (EDS) analysis was performed at selected positive x. Figure 4(c) shows the measurements carried out on the film at $x = +5$ mm from the center. Three spots (1–3) were evaluated and the average counts are shown in the inset of Fig. 4(d). Figure 4(d) shows the EDS spectra of the Cu_2S film obtained at different x. As observed, the thicker film at $x = +15$ mm exhibits only the characteristic x-ray peaks located at 0.93, 8.04, and 2.31 keV expected for the Cu $L\alpha$, Cu $K\alpha$ and S $K\alpha$,

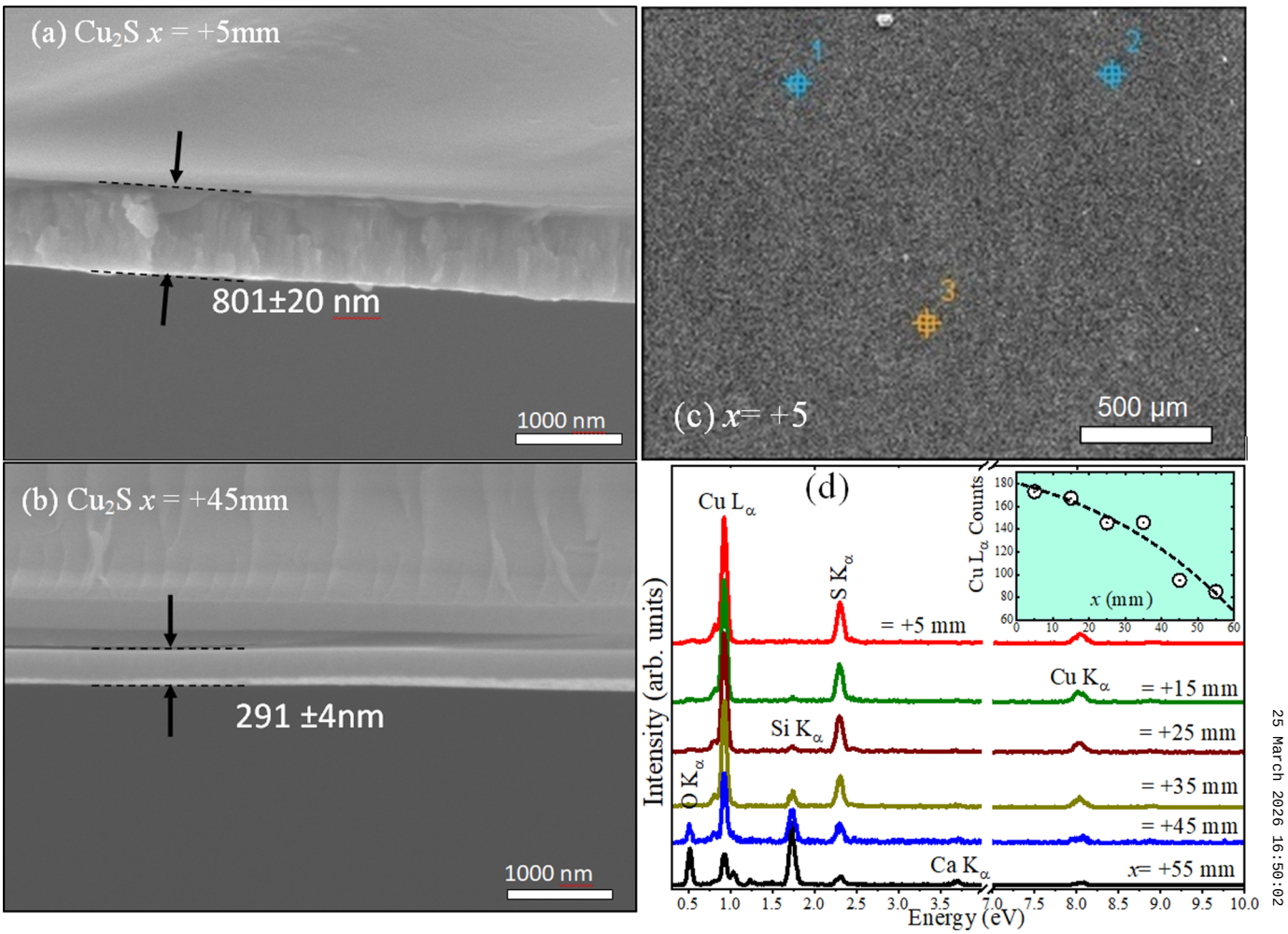

FIG. 4. Cross-sectional SEM micrographs of the Cu_2S films located at different distances (a) $x = +5$ mm, and (b) $x = +45$ mm. (c) Surface image of the film at $x = +5$ mm, showing the three evaluated spots. (d) EDS of the Cu_2S film located at different x. The inset exhibits the reduction of the counts of the Cu $L\alpha$ peak as x increases, suggesting a reduction of the Cu quantity as the film moves away from the center.

respectively. This result confirms the chemical composition of the Cu_2S film. However, the thinner film located at $x = +55$ mm shows additional characteristic x-ray peaks at 0.53, 1.74, and 3.69 keV, respectively, which are associated with the O $K\alpha$, Si $K\alpha$, and Ca $K\alpha$, coming from the chemical composition of the borosilicate glass substrate. The latter result is associated with the reduction of the film thickness, and it is evidenced by the reduction of the counts of the Cu $L\alpha$ peak as x increases [see the inset in Fig. 4(d)].

3. Optical properties

To assess the optical properties of the as-grown film, ultraviolet–visible (UV–Vis) spectroscopy measurements were carried out in the wavelength (λ) range from 110 to 1100 nm. The optical spectra were recorded in transmittance mode, sweeping the wavelength range four times while rotating the sample by 90° after each measurement in order to improve accuracy. The transmittance spectra of the Cu_2S thin film at different x are collected in Figs. 5(a) and 5(b) and represented by solid symbols. Additionally, the spectrum of the borosilicate substrate (open black symbols) is included in each panel. In order to simulate the transmittance spectra of the air/substrate/film/air layers in the UV–Vis region, SpectraRay/4 software from SENTECH was used. This software implements the soda lime float glass (SLG) with tin impurities and the combination of the Tauc–Lorentz oscillators (TLOs) and Drude models to the borosilicate glass layers (1 mm) and Cu_2S thin films, respectively.[21] In Figs. 5(a) and 5(b) are shown the simulated and experimental data. As observed, a good match between the experimental data (symbols) and the simulated curves (solid red lines) was obtained. Regarding the transmittance maxima (TM), as can

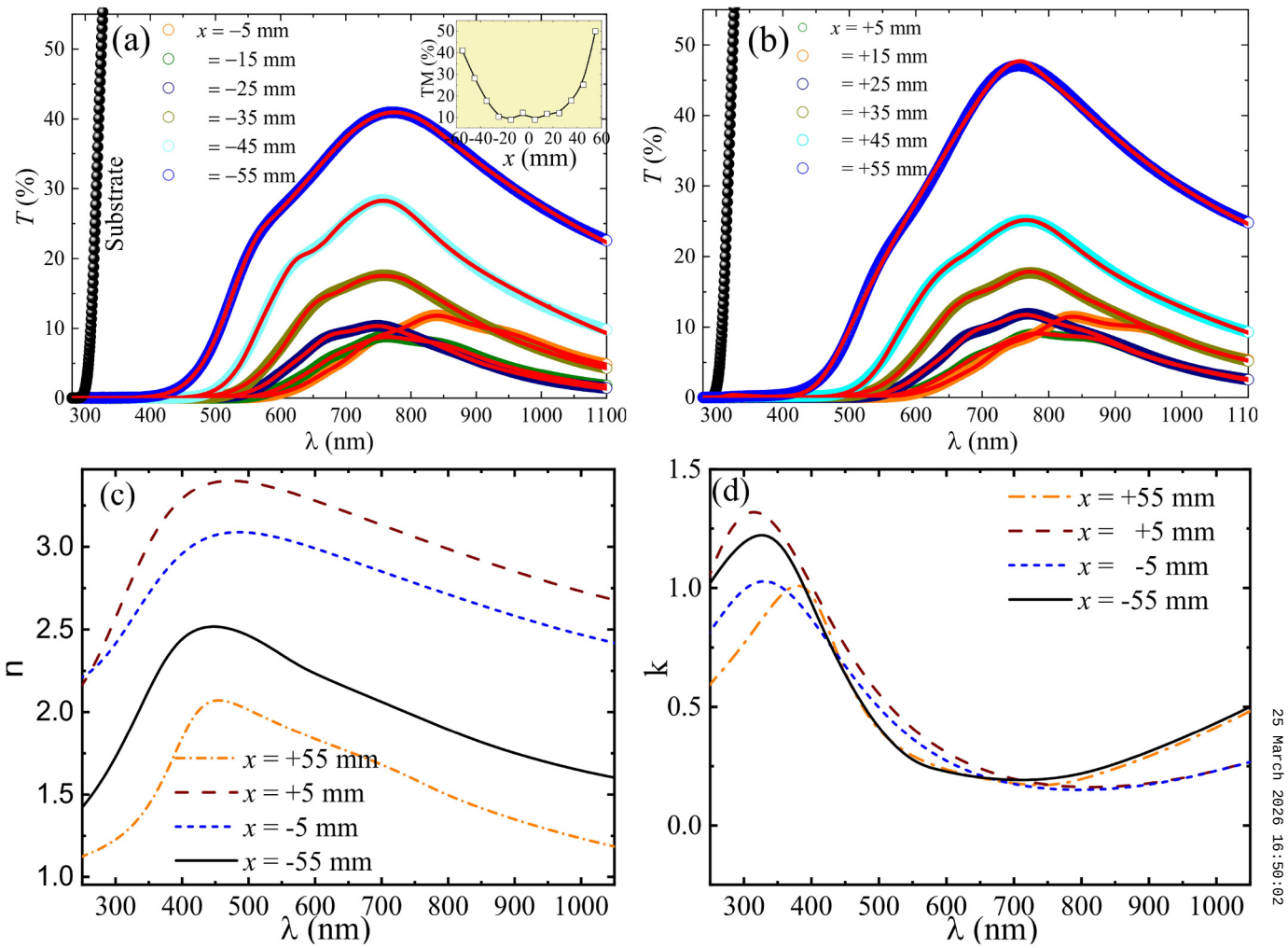

FIG. 5. (a) and (b) Room-temperature transmittance spectra of Cu_2S thin film collected at different x. The transmittance spectrum of the glass substrate (filled circles) is included for comparison purposes. Simulated spectra are represented by the solid red lines. In the inset, the transmittance maxima (TM) as a function of the sample position is included. (c) Refractive index and (d) extinction coefficient curves as a function of the wavelength, plotted for some representative x (−55, −5, +5, and +55 mm).

be seen in the inset of Fig. 5(a), the thinner region of the film displays more transparency. Inversely, the thicker region of the film, located around the center of the substrate, displays lower transparency. It is worth noting that the transparency of a thin film scales linearly with the optical path length difference (OPD) of the light traveling through it. Light is increasingly absorbed in thicker films as the OPD expands, which leads to a transparency reduction as the film thickness increases.

The TLO model has been successfully used to simulate the optical transmittance of materials, particularly in the determination of the energy bandgap and the absorption edge, which describes how a material's absorption coefficient (α) changes with the photon energy ($h\nu$), as in the case of TiO_2/SnO_2 thin films.[22] Meanwhile, the Drude model, which describes the behavior of free electrons in a material, that is associated with the free electron density, electron mass, and relaxation time, has been successfully used to model metals[23] and transparent conductive oxides (TCOs).[24,25] In Fig. 6(a) are plotted the film thickness extracted from XRD and optical data analyses. In addition, to validate our results, two film thickness values (star symbols) obtained from SEM cross-section images were included. As observed our results a good show of consistency [see Fig. 6(a)]. Figure 6(b) shows the refractive index (n) and extinction coefficient (k) as a function of the film thickness (t_T), the latter extracted from the n and k curves vs λ, as shown in Figs. 5(c) and 5(d). On the other hand, n increases substantially as t_T increases, whereas k slightly decreases as t_T increases, as shown in Fig. 6(b). The refractive index trend with the film thickness can be explained based on the photoelastic

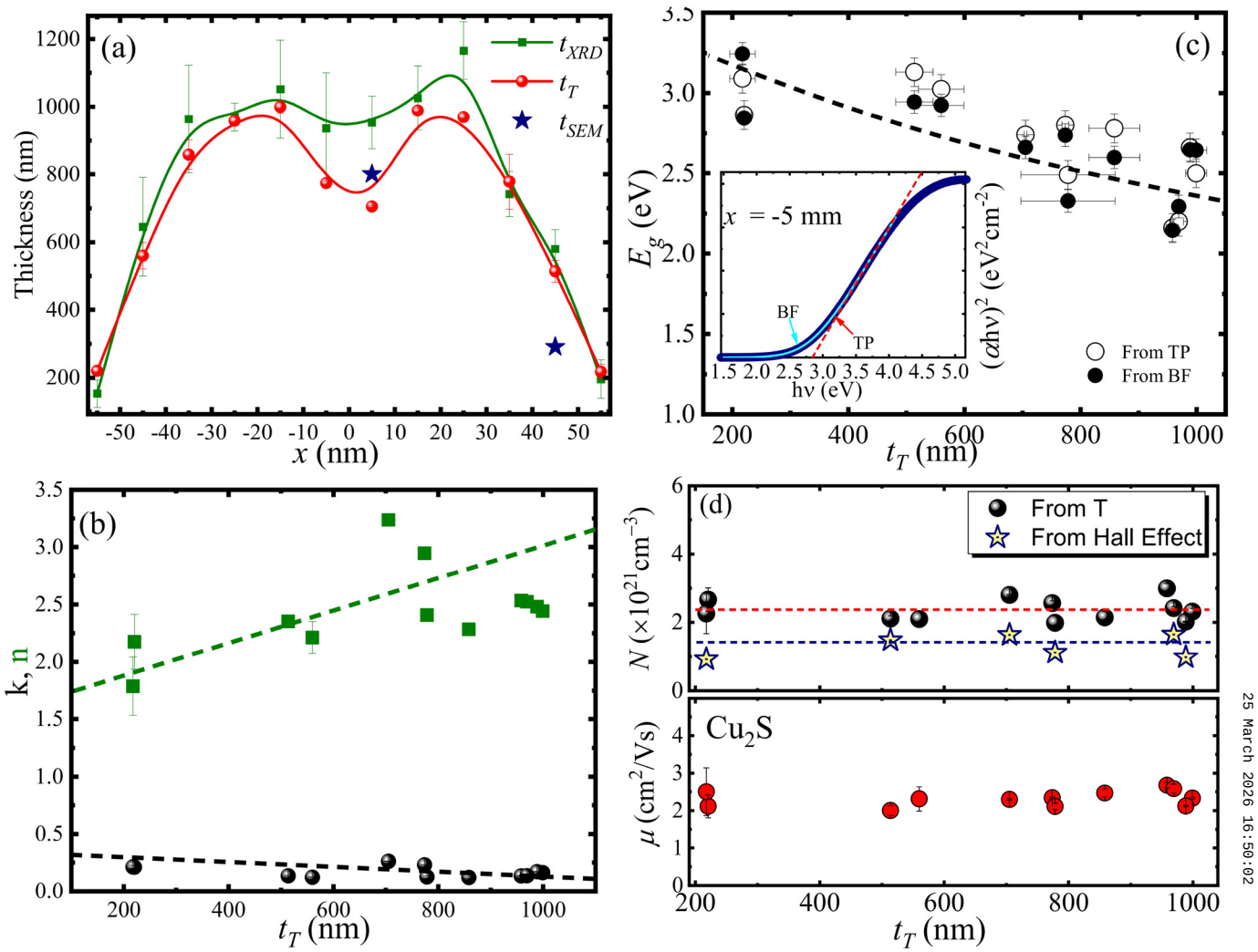

FIG. 6. (a) Film thickness obtained from XRD (t_{XRD}), transmittance (t_T), and cross-section SEM images (t_{SEM}) as a function of x. (b) Refractive index (n) and extinction coefficient (k) as a function of t_T. (c) Energy bandgap vs t_T determined from the Tauc plot (TP) and the band-fluctuation (BF) models. (d) Charge carrier concentration (upper panel) and hole mobility (lower panel) as a function of t_T. Here, the $m_e^* = 0.8\, m_e$ (from Ref. 30) is used for the N values determination.

effect. This effect is expected to occur when a material experiences mechanical stress, leading to changes in the optical properties, including the refractive index.[26,27] In the case of compressive strain, a reduction in the material dimensions is expected, reducing the bond distance between the ions. In some materials, such as in KBr, NaCl, LiF, diamond, and quartz, the change in refractive index due to a compressive strain is generally positive, meaning that the refractive index increases with the strain. However, in other materials, such as MgO and Al_2O_3, the refractive index decreases.[27] In the case of Cu_2S, our finding suggests a decreasing tendency of the refractive index with the compressive strain.

Absorption edges in the wavelength (λ) region from 450 to 550 nm [see Figs. 5(a) and 5(b)] are associated with the optical bandgap energy (E_g). The latter can be assessed via the absorption coefficient (α) obtained from the relation: $\alpha = 4\pi k/\lambda$. E_g is commonly determined from the intercept of the linear portion of $(\alpha h\nu)^2$ vs $(h\nu)$ plot using the Tauc plot-like (TP) method, i.e., $(\alpha h\nu) = A(h\nu - E_g)^n$, considering $n = 1/2$ for direct electronic transitions. However, this method does not account for the Urbach tail, which can be present in both degenerate and non-degenerate semiconductors. In order to include this contribution, the band-fluctuation (BF) model was used and is described by[28]

$$\alpha(h\nu) = (1/2)(A_0/h\nu)\sqrt{\pi/\beta}\, Li_{1/2}\left(-e^{\beta(h\nu - E_g)}\right). \quad (3)$$

Here, $h\nu$ is the photon energy, A_0 is a constant in units of $eV^{-1}\,cm^{-1}$, β is the inverse of Urbach energy, and $Li_j(x)$ is the jth order polylogarithm function of x. Typical fits for both methods (TP and BF) are presented in the inset of Fig. 6(c) for the film spot at $x = -5$ mm.

The bandgap values obtained from both methods as a function of the film thickness show a decreasing trend, as shown in Fig. 6(c). A plausible explanation for the bandgap closing could be assigned to the grain size effect once the crystallite radius within the as-grown Cu_2S film displays a tendency to decrease from ~12 to ~8 nm (see Table I). The lower end is close to the Bohr radius (3–5 nm) of $Cu_{2-x}S$, reported in the literature.[29] The Urbach energy obtained from the BF fitting displays a tendency to increase from 0.2 to 0.4 meV as the film thickness increases. That Urbach energy increase is likely associated to the structural disorder, which is in turn associated with the size effect. The latter leads to a broader absorption tail in the absorption spectrum, which results in a higher Urbach energy. Regarding the free carrier density (N) and carrier mobility (μ), both can be determined from the strength (ω_p) and damping (ω_τ) frequencies via the relations $\omega_p = \sqrt{Ne^2\epsilon_0 m^*}$ and $\omega_\tau = e/\mu m^*$,[25] where ϵ_0 is the permittivity of free space, m^* is the effective mass of the carriers ($0.8\,m_e$),[30] and e is the electron charge. As shown in the upper panel of Fig. 6(d), the charge carrier density (N) values are in the range of 2×10^{21} to $4 \times 10^{21}\,cm^{-3}$, which are in the region of the expected values reported in the literature.[3] The effective mass of the holes can be estimated from the $m^* = Ne^2/\omega_p^2\epsilon_0$ relationship, utilizing the experimentally N (obtained from Hall effect measurements). This analysis yields an effective mass value of $0.45 \pm 0.08\,m_e$. Notably, this value is lower than the one reported in Ref. 30. The discrepancy could potentially be attributed to various factors. For instance, N is in the order of $10^{21}\,cm^{-3}$, suggesting that the parabolic band approximation might not be longer valid. Additionally, intrinsic defects, low dimensions of the crystallites, and lattice strain can change the electronic band structure, modifying the curvature of bands near the edges. Meanwhile, as shown in the lower panel of Fig. 6(d), the assessed mobility (μ) displays values in the range of 2–3 $cm^2/V\,s$, in good agreement with the $2\,cm^2/V\,s$ reported in Ref. 31.

4. DC electrical properties

To assess the electrical transport properties of the Cu_2S polycrystalline film, the Van der Pauw configuration was used to evaluate sheet resistance (SR) and charger carrier concentration (N), at room temperature. Figure 7(a) shows the sheet resistance (SR) as a function of the film thickness (t), as obtained from both the XRD and transmittance data analyses. As expected, the sheet resistance decreases from ~60 to ~10 Ω/ while increasing the film thickness. Meanwhile, the resistivity of the Cu_2S film shows values in the range of $\sim 0.79 \times 10^{-3}$ to $\sim 1.90 \times 10^{-3}\,\Omega$ cm, which are in good agreement with those reported in the literature ($\sim 0.14 \times 10^{-3}$ to $\sim 3.0 \times 10^{-3}\,\Omega$ cm).[32] The Hall effect was used to estimate the carrier charge concentration. In this regard, ohmic contact for the metal/semiconductor (indium/copper sulfide) contact interface was achieved; the metal presenting a work function of $\phi_{In} = 4.12$ eV,

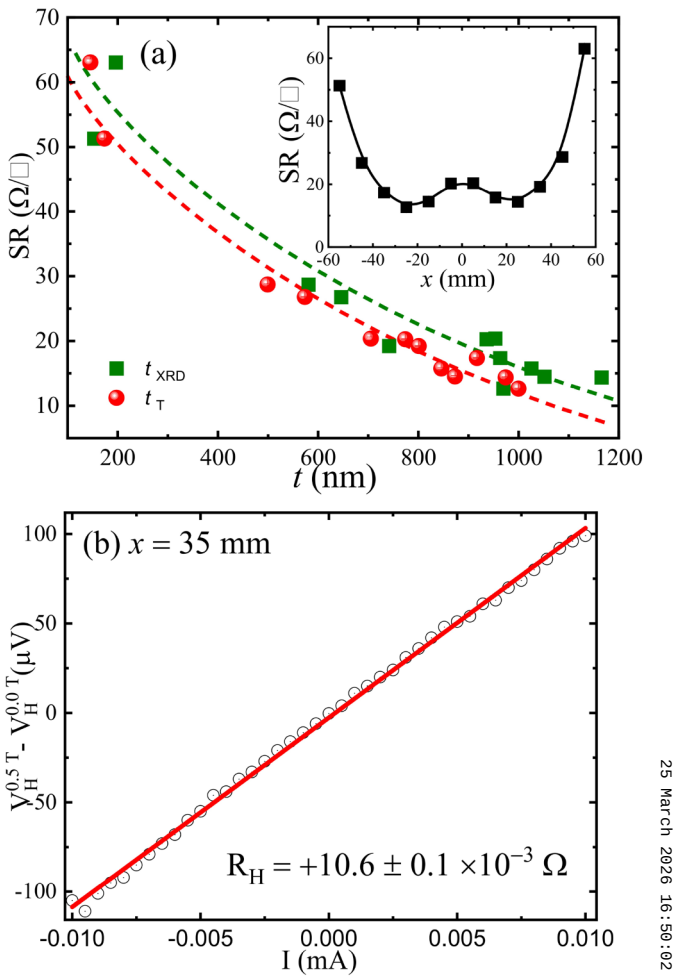

FIG. 7. Sheet resistance (SR) as a function of the thickness (t) obtained from both the XRD (solid green squares) and from the transmittance (solid red circles) data analyses. Dashed green and red lines are only a guide to the eyes. In the inset of (a) is displayed the SR as a function of x. (b) The Hall voltage measurement in a magnetic field and with no magnetic field ($V_H^{0.5T}$–$V_H^{0.0T}$) as a function of the applied current, I. The solid red line represents the linear fit performed in order to extract the Hall resistance.

which is lower than the work function of the semiconductor sample (Cu_2S) ($\phi_{Cu_2S} = 4.82$ eV). Figure 7(b) displays the difference between the voltage measured with an applied magnetic field of $H = 0.515$ T and the voltage measured with $H = 0$ T, ($V_H^{0.5T}$–$V_H^{0.0T}$) as a function of the current (I), from which the Hall resistance (R_H) was extracted. As it is displayed in Fig. 7(b), the linear behavior evidences the achieved ohmic contact metal/semiconductor, whereas the positive sign reveals a p-type semiconductor. The values of N are in the range of 0.92×10^{21}–$1.65 \times 10^{21}\,cm^{-3}$, with no clear tendency with the film thickness [see Fig. 6(d)], but in very good agreement with the values reported in the literature.[3,33]

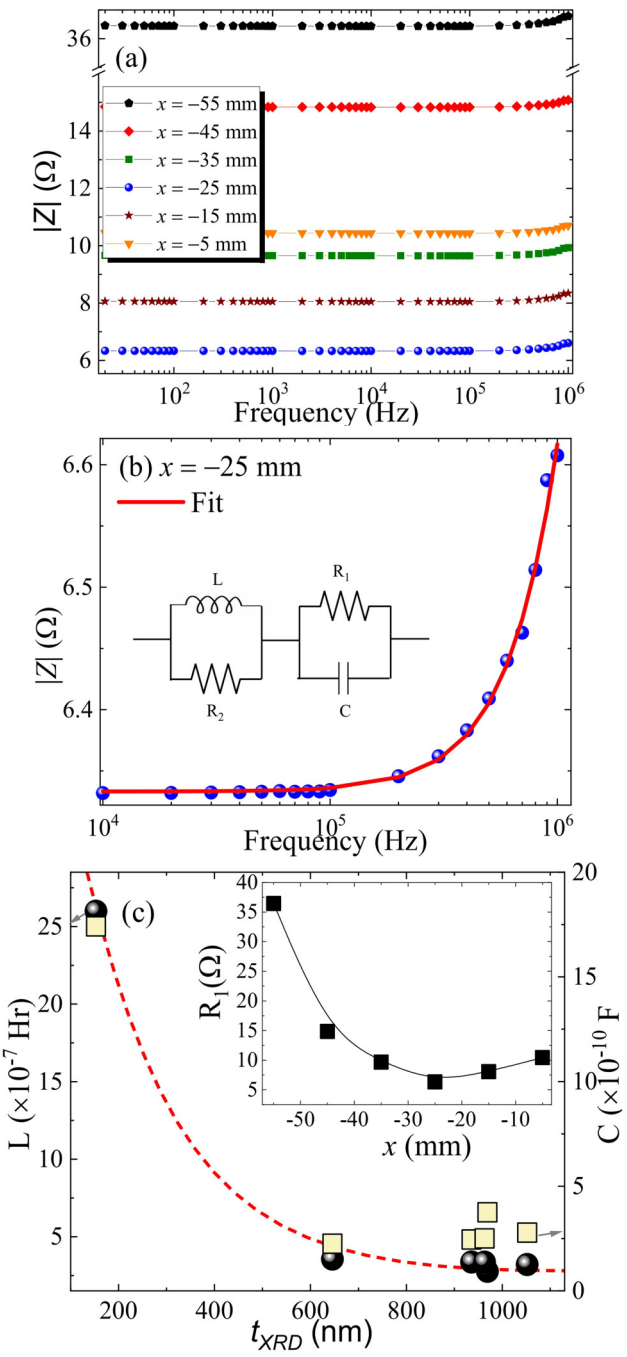

FIG. 8. (a) Total impedance $|Z|$ vs frequency (from 20 Hz to 1 M Hz) for the Cu_2S polycrystalline film at different x from −5 to −55 mm. (b) Typical fit of the $|Z|$ vs frequency curve corresponding to $x = -25$ mm using the RL–RC equivalent circuit. Symbols are experimental values and the solid red line is the best fit. (c) Inductance (solid black balls) and capacitance (solid yellow squares) of the RL–RC equivalent circuit obtained from the analyses. The dashed red line is a guide to the eyes. The inset displays the R_1 vs x. The solid black squares are experimental values whereas the solid black line is a guide to the eyes.

5. AC electrical properties

In order to perform AC electrical characterization of the Cu_2S polycrystalline film, the real (Z') and imaginary (Z'') impedances were recorded at room temperature. The recorded data are expected to reveal the underlying physical processes governing the behavior of the Cu_2S film, such as charge carrier trapping and recombination, interface effects, and the impact of defects or impurities on device performance. This understanding can guide the design and engineering of better devices. Figure 8(a) shows the total impedance $|Z| = \sqrt{Z'^2 + Z''^2}$ as a function of the operating frequency for the Cu_2S film at different x, from $x = -5$ mm to $x = -55$ mm. A nearly flat behavior is observed in the frequency range from 20 Hz to 0.1 MHz, suggesting the presence of an inductive component. All curves shown in Fig. 8(a) were fitted in order to obtain the total AC impedance response, being well modeled with a parallel-resistor–inductor in series with a parallel-resistor–capacitor circuit (RL–RC circuit), as schematically shown in the inset of Fig. 8(b). Herein, the impedance of the RL parallel branch is given by $Z_{RL} = 1/(R + j\omega L)$. Meanwhile, the impedance of the RC parallel branch is given by $Z_{RC} = 1R/(R + j\omega RC)$. The total impedance of this circuit is the sum of these two impedances connected in series, i.e., $Z = Z_{RL} + Z_{RC}$. The total inductive response was modeled using the EIS (Electrochemical Impedance Software) analyzer program.[34] A typical fit is shown in Fig. 8(b) for the Cu_2S film at $x = -25$ mm. The inductance (L) and capacitance (C) obtained from the analyses show a dependence on the film thickness as shown in Fig. 8(c). It is observed that both parameters rise as the film thickness decreases. This behavior can be attributed to the specific properties and geometry of the films. The capacitance increase must be related to a closing of the load store in the thinner films. Concerning the inductance, a decrease in the film thickness may result in a more tightly coiled electrical circuit. Because inductance is proportional to the number of turns and the cross-sectional area, increasing the number of turns within a thinner film can increase the inductance. In addition, as shown in the inset of Fig. 8(c), the trend of R_1 with the film thickness shows the same trend determined for the sheet resistance, suggesting the validity of the model. Meanwhile, the resistor parallel to the inductance component (R_2) displays values between 29 and 50 Ω, with no clear tendency with the film thickness.

IV. CONCLUSIONS

In conclusion, in this study, copper sulfide thin films on borosilicate glass were grown by the DC magnetron sputtering method. Results revealed the formation of only hexagonal Cu_2S phase for all films. A strong dependence of unit cell volume, mean crystallite size, and film thicknesses on the substrate position was determined. This correlation is attributed to the observed thickness gradient, with the substrate positioned farther toward the center showing a significant impact on these parameters. The film's thickness as a function of the substrate's center point (x) was successfully and consistently determined via x-ray diffraction and optical transmittance data analyses. While x-ray diffraction is not commonly employed for thickness determination, the innovative approach presented in this study proves to be valuable in precisely assessing the film thickness. Those results were corroborated via cross-

sectional scanning electron microscopy images. In addition, the transmittance approach to assess the film's thickness was also employed via refractive index (n) and the extinction coefficient (k), which increases and decreases with the film thickness, respectively. These findings were associated with the compressive strain effect, which is stronger for thinner films due to the shrinking of the unit cell volume as the film thickness decreases. Electrical resistivity ($\sim 0.79 \times 10^{-3}$– $\sim 1.90 \times 10^{-3}\,\Omega$ cm) and charge carrier concentrations (N) $\sim 0.92 \times 10^{21}$–$1.65 \times ^{21}$ cm^{-3} were determined for the as-grown Cu_2S film. The N values derived from the Hall effect were cross-validated through optical measurements employing the Drude model. Remarkably, these values exhibited a robust consistency, reinforcing the reliability of our findings. The equivalent RL–RC circuit proposed to model the total impedance as a function of the frequency allows one to extract the key electrical properties of the film, showing that the as-grown Cu_2S films can be used for electronic applications. The results suggest that the as-grown Cu_2S films exhibit promising optoelectrical characteristics, making them suitable for electronic applications. Overall, this research provides valuable insights into the controlled growth and electrical properties of copper sulfide thin films, paving the way for their potential applications in optoelectronic devices.

ACKNOWLEDGMENTS

This research was funded by the Peruvian National Program for Scientific Research and Advance Studies (ProCiencia), Grant No. PE-501078343-2022- PROCIENCIA. J. A. Guerra, P. Llontop, and F. Aragón acknowledge the support of the Pontificia Universidad Católica del Perú (PUCP) vice chancellorship for research (VRI, Project No. CAP-PI0997), Science Department, and the Center for Characterization of Materials (CAM) at PUCP.

AUTHOR DECLARATIONS

Conflict of Interest

The authors have no conflicts to disclose.

Author Contributions

J. R. Velasquez Ordoñez: Investigation (equal); Writing – review & editing (equal). **J. Rivera-Taco:** Formal analysis (equal); Funding acquisition (equal); Writing – review & editing (equal). **D. G. Pacheco-Salazar:** Data curation (equal); Writing – review & editing (equal). **J. A. H. Coaquira:** Data curation (equal); Writing – review & editing (equal). **J. L. Maldonado:** Data curation (equal); Writing – review & editing (equal). **J. A. Guerra:** Data curation (equal); Funding acquisition (equal); Writing – original draft (equal); Writing – review & editing (equal). **P. Llontop:** Data curation (equal); Writing – review & editing (equal). **P. C. Morais:** Data curation (equal); Writing – original draft (equal); Writing – review & editing (equal). **F. F. H. Aragón:** Conceptualization (equal); Data curation (equal); Formal analysis (equal); Investigation (equal); Supervision (equal); Writing – original draft (equal); Writing – review & editing (equal).

DATA AVAILABILITY

The data that support the findings of this study are available from the corresponding author upon reasonable request.

REFERENCES

[1]P. Savage, R. Georg, R. Armytage, H. Williams, and A. Halliday, "Silicon isotope homogeneity in the mantle," Earth Planet. Sci. Lett. **295**, 139–146 (2010).
[2]L. Zong, B. Zhu, Z. Lu, Y. Tan, Y. Jin, N. Liu, Y. Hu, S. Gu, J. Zhu, and Y. Cui, "Nanopurification of silicon from 84% to 99.999% purity with a simple and scalable process," Proc. Natl. Acad. Sci. U.S.A. **112**, 13473–13477 (2015).
[3]P. Parreira, G. Lavareda, A. Amaral, A. Botelho do Rego, O. Conde, J. Valente, F. Nunes, and C. Nunes de Carvalho, "Transparent p-type Cu_xS thin films," J. Alloys Compd. **509**, 5099–5104 (2011).
[4]M. Patil, D. Sharma, A. Dive, S. Mahajan, and R. Sharma, "Synthesis and characterization of Cu_2S thin film deposited by chemical bath deposition method," Procedia Manuf. **20**, 505–508 (2018), *2nd International Conference on Materials, Manufacturing and Design Engineering (iCMMD2017)*, 11–12 December 2017, MIT Aurangabad, Maharashtra, India.
[5]R. A. Ismail, A.-M. E. Al-Samarai, and A. M. Muhammed, "High-performance nanostructured p-Cu_2S/n-Si photodetector prepared by chemical bath deposition technique," J. Mater. Sci.: Mater. Electron. **30**, 11807–11818 (2019).
[6]F. Zhao, X. Chen, N. Xu, P. Lu, J.-G. Zheng, Q. Su, and M. Wu, "Controlled growth of Cu_2S hexagonal microdisks and their optical properties," J. Phys. Chem. Solids **67**, 1786–1791 (2006).
[7]H. K. Kaplan, S. K. Akay, S. Pat, and M. Henini, "p-type transparent Cu_2S thin film grown by thermionic vacuum arc for optoelectronic applications," Mater. Sci. Eng. B **263**, 114872 (2021).
[8]G. A. Armantrout, D. E. Miller, K. E. Vindelov, and T. G. Brown, "Formation of thin Cu_2S (chalcocite) films using reactive sputtering techniques," J. Vac. Sci. Technol. **16**, 212–215 (1979).
[9]Y. He, W. Kriegseis, J. Bläsing, A. Polity, T. Krämer, D. Hasselkamp, B. Meyer, M. Hardt, and A. Krost, "(001)-textured Cu_2S thin films deposited by RF reactive sputtering," Jpn. J. Appl. Phys. **41**, 4630 (2002).
[10]S. Swann, "Film thickness distribution in magnetron sputtering," Vacuum **38**, 791–794 (1988).
[11]Y. B. Guillen-Baca, C. A. V. Huayhua, K. J. P. Corrales, A. F. Carlos-Chilo, F. F. H. Aragón, M. C. Mathpal, S. W. da Silva, J. A. H. Coaquira, W. Sucasaire, J. A. Guerra, and D. G. Pacheco-Salazar, "Lattice strain effects on the structural properties and band gap tailoring in columnarly grown Fe-doped SnO_2 films deposited by DC sputtering," J. Phys. D: Appl. Phys. **52**, 465306 (2019).
[12]F. Aragón, J. Aquino, N. Gomes, J. Ardisson, S. da Silva, D. Pacheco-Salazar, and J. Coaquira, "Characterization of polycrystalline SnO_2 films deposited by DC sputtering technique with potential for technological applications," J. Eur. Ceram. Soc. **37**, 3375–3380 (2017).
[13]G. Zoppi, N. Beattie, J. Major, R. Miles, and I. Forbes, "Electrical, morphological and structural properties of RF magnetron sputtered Mo thin films for application in thin film photovoltaic solar cells," J. Mater. Sci. **46**, 4913 (2011).
[14]C. Srinivasan, S. Pattanaik, C. Balasingh, A. Singh, and N. A. L. of India, "Measurement of thickness of thin films by the x-ray diffraction method," NAL Technical Note (National Aeronautical Laboratory, 1979).
[15]B. Toby, "EXPGUI, a graphical user interface for GSAS," J. Appl. Cryst. **34**, 210–213 (2001).
[16]R. Cava, F. Reidinger, and B. Wuensch, "Mobile ion distribution and anharmonic thermal motion in fast ion conducting Cu_2S," Solid State Ionics **5**, 501–504 (1981), Proceedings of the International Conference on Fast Ionic Transport in Solids.
[17]A. L. Patterson, "The Scherrer formula for x-ray particle size determination," Phys. Rev. **56**, 978–982 (1939).
[18]T. Giraldi, M. Escote, M. Bernardi, V. Bouquet, E. Leite, E. Longo, and J. Varela, "Effect of thickness on the electrical and optical properties of Sb doped SnO_2 (ATO) thin films," J. Electroceram. **13**, 159–165 (2004).

[19]T. A. Hameed, A. R. Wassel, and I. El Radaf, "Investigating the effect of thickness on the structural, morphological, optical and electrical properties of $AgBiSe_2$ thin films," J. Alloys Compd. **805**, 1–11 (2019).
[20]T. Stein, see https://xraytools.com/ for "Absorption Coefficient Calculator" (2019).
[21]C. Bohórquez-Martínez, H. Bakkali, J. Delgado, E. Blanco, M. Herrera, and M. Dominguez, "Spectroscopic ellipsometry study on tuning the electrical and optical properties of Zr-doped ZnO thin films grown by atomic layer deposition," ACS Appl. Electron. Mater. **4**, 925 (2022).
[22]S. De la Torre Pari, J. Aquino, A. Carlos-Chilo, J. Guerra, J. Coaquira, D. Pacheco-Salazar, J. Felix, J. Solis, and F. Aragón, "Enhancing the photoconductivity and gas sensing performance of TiO_2/SnO_2 heterostructures tuned by the thickness of the SnO_2 upper layer," Appl. Surf. Sci. **613**, 156028 (2023).
[23]A. D. Rakić, A. B. Djurišić, J. M. Elazar, and M. L. Majewski, "Optical properties of metallic films for vertical-cavity optoelectronic devices," Appl. Opt. **37**, 5271–5283 (1998).
[24]Z. Wang, C. Chen, K. Wu, H. Chong, and H. Ye, "Transparent conductive oxides and their applications in near infrared plasmonics," Phys. Status Solidi A **216**, 1700794 (2019).
[25]P. Llontop, C. E. Torres, M. Piñeiro, L. Conde, A. Tejada, J. A. Töfflinger, F. Rumiche, F. F. H. Aragón, D. G. Pacheco-Salazar, R. Grieseler, L. Korte, and J. A. Guerra, "Indirect excitation and luminescence activation of Tb doped indium tin oxide and its impact on the host's optical and electrical properties," J. Phys. D: Appl. Phys. **55**, 210002 (2022).
[26]D. F. Nelson and M. Lax, "Theory of the photoelastic interaction," Phys. Rev. B **3**, 2778–2794 (1971).
[27]R. Waxler and C. Weir, "Effect of hydrostatic pressure on the refractive indices of some solids," J. Res. Natl. Bur. Stand. **69A**, 325–333 (1965).
[28]J. A. Guerra, A. Tejada, L. Korte, L. Kegelmann, J. A. Töfflinger, S. Albrecht, B. Rech, and R. Weingärtner, "Determination of the complex refractive index and optical bandgap of $CH_3NH_3PbI_3$ thin films," J. Appl. Phys. **121**, 173104 (2017).
[29]Y. Zhao, H. Pan, Y. Lou, X. Qiu, J. Zhu, and C. Burda, "Plasmonic $Cu_{2-x}S$ nanocrystals: Optical and structural properties of copper-deficient copper(I) sulfides," J. Am. Chem. Soc. **131**, 4253–61 (2009).
[30]A. Sheardy and D. M. Arvapalli, "Novel microwave synthesis of near-metallic copper sulfide nanodiscs with size control: Experimental and dft studies of charge carrier density," Nanoscale Adv. **2**, 1054 (2020).
[31]R. E. Agbenyeke, B. K. Park, T.-M. Chung, C. G. Kim, and J. H. Han, "Growth of Cu_2S thin films by atomic layer deposition using $Cu(dmamb)_2$ and H_2S," Appl. Surf. Sci. **456**, 501–506 (2018).
[32]M. Adelifard, H. Eshghi, and M. M. B. Mohagheghi, "An investigation on substrate temperature and copper to sulphur molar ratios on optical and electrical properties of nanostructural CuS thin films prepared by spray pyrolysis method," Appl. Surf. Sci. **258**, 5733–5738 (2012).
[33]M. Ramya and S. Ganesan, "Role of thickness in physical properties of Cu_2S thin films prepared by vacuum evaporation method," J. Optoelectron. Adv. Mater. **14**, 910–917 (2012); available at https://joam.inoe.ro/articles/role-of-thickness-in-physical-properties-of-cu2s-thin-films-prepared-by-vacuum-evaporation-method/fulltext.
[34]A. S. Bondarenko and G. A. Ragoisha, *EIS Spectrum Analyser* (2008); available at http://www.abc.chemistry.bsu.by/vi/analyser